Phase transitions of wave packet dynamics in disordered non-Hermitian systems

Helene Spring[1*], Viktor Könye[2], Fabian A. Gerritsma[1],
Ion Cosma Fulga[2] and Anton R. Akhmerov[1]

1 Kavli Institute of Nanoscience, Delft University of Technology,
P.O. Box 4056, 2600 GA Delft, The Netherlands
2 Institute for Theoretical Solid State Physics, IFW Dresden
and Würzburg-Dresden Cluster of Excellence ct.qmat,
Helmholtzstr. 20, 01069 Dresden, Germany

⋆ helene.spring@outlook.com

Abstract

Disorder can localize the eigenstates of one-dimensional non-Hermitian systems, leading to an Anderson transition with a critical exponent of 1. We show that, due to the lack of energy conservation, the dynamics of individual, real-space wave packets follows a different behavior. Both transitions between localization and unidirectional amplification, as well as transitions between distinct propagating phases become possible. The critical exponent of the transition is close to 1/2 in propagating-propagating and (de)localization transitions.

Contents

1   Introduction

Wave propagation in a strongly disordered medium stops due to Anderson localization [1]. The latter depends only on macroscopic properties of the medium, such as its dimensionality, symmetries, and topological invariants. In one space dimension (1D), for instance, generic disorder will localize all eigenstates, even if the disorder strength is infinitesimally weak. On the other hand, weak anti-localization becomes possible in two- and higher-dimensional systems, depending on their symmetries [2]. In such cases, the full spectrum of a disordered energy-conserving medium contains regions of localized and extended states, which are separated by mobility edges.

Unlike energy-conserving media, non-Hermitian systems with point gaps can exhibit fundamentally different behaviors in the presence of disorder. For instance, in the absence of energy conservation, it was found that weak disorder does not localize all states, even in 1D systems [3, 4]. Instead, similar to their higher-dimensional Hermitian counterparts, in 1D non-Hermitian systems localized and delocalized eigenstates are separated by mobility edges across which the localization length diverges. A recent work has shown that this divergence is governed by a universal critical exponent taking the value $\nu = 1$ [5].

One of the practical uses of the theory of eigenstate localization is to predict the dynamics of individual wave packets. In Hermitian systems, this is straightforward: the initial wave packet is decomposed into a superposition of states with different energies. The wave packet components above the mobility edge diffuse through the medium, while those below the mobility edge stay localized. By contrast, non-Hermitian systems break energy conservation, such that it is no longer possible to directly describe the wave packet dynamics by separating it into components with different energies.

Here we demonstrate that the difference between single energies and wave packets is profound. Because in the long-time limit any wave packet in a system with a point gap converges to a maximally amplified waveform, the asymptotic shape of the wave packet may change discontinuously when the system parameters are varied. This enables a metal-metal transition between different unidirectionally amplified phases in addition to the previously known localization transition. Furthermore, in finite-size systems the fluctuations of the maximally amplified energy are self-averaging, which results in a critical exponent $\nu \approx 1/2$ that is close to our analytical estimate of $1/2$.

The structure of the manuscript is as follows. In Sec. 2 we demonstrate the universal convergence of wave packets in weakly disordered systems to the maximally amplified waveform. In Sec. 3 we study the transition between distinct propagating phases. In Sec. 4 we show that the wave packet single-frequency transition differs from the static non-Hermitian single-frequency transition. We conclude in Sec. 5.
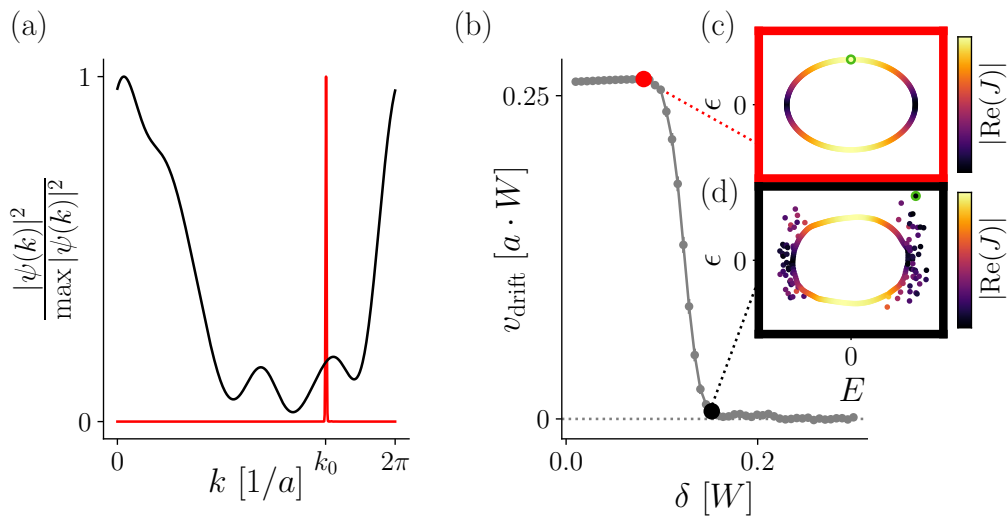
Figure 1: Maximally amplified waveforms of disordered Hatano-Nelson systems Eq. (1), with disorder in units of the model bandwidth W. Random disorder terms $U_{i,j}$ with $i \in \{0, 1, 2\}$ and j the site number (1) are sampled from distributions with standard deviation δ_i. We set $\delta_0 = \delta_1 = \delta_2 \equiv \delta$. (a) Magnitude of the Fourier components $|\psi(k)|^2$ of a wave packet evolved under H_{HN} for $\delta = 0.01$ (red) and $\delta = 0.3$ (black). The maximally amplified Fourier component of the system with low disorder is marked by k_0. (b) The average drift velocity v_{drift} as a function of disorder strength δ, and a the lattice constant. (c) Eigenvalues of H_{HN} for a single disorder realization with disorder strength $\delta = 0.08$. The point of maximal amplification ϵ_{max} is highlighted with green. (d) Eigenvalues of a disordered system with disorder $\delta = 0.15$. ϵ_{max} is highlighted in green. Plot details in App. A.

2 Maximally amplified wave packet

Unlike their Hermitian counterparts, one-dimensional (1D) non-Hermitian systems with no symmetries do not localize in the presence of weak disorder [3, 6, 7]. The different Fourier components of the wave packet, which are coupled by scattering events, are amplified at different rates, depending on the value of ϵ, the imaginary part of their energy $E + i\epsilon$ [4]. The eigenstate whose eigenvalue has the largest positive imaginary component, ϵ_{max}, is amplified the fastest. This means that any waveform in a weakly disordered medium converges to the maximally amplified waveform, forming an envelope in Fourier space around the point of maximal amplification k_0.

To demonstrate this we consider a Hatano-Nelson Hamiltonian [3]:

$$H_{\mathrm{HN}} = \sum_j U_{0,j}|j\rangle\langle j| + \left(-\frac{W}{2}e^{-h} + U_{1,j}\right)|j\rangle\langle j+1| + \left(-\frac{W}{2}e^{h} + U_{2,j}\right)|j+1\rangle\langle j|, \quad (1)$$

where the sum runs over sites j of the system, W is a hopping parameter that sets the bandwidth of the system, h fixes the magnitude of the hopping asymmetry, and $U_{k,j}$ are the complex disorder coefficients whose real and imaginary parts are independently sampled from a normal distribution with zero mean and standard deviation δ_k. Thus, δ_k models the strength of each type of disorder (onsite or hopping).

We time-evolve wave packets numerically by Taylor expanding the time-dependent Schrösodinger equation to first order [See App. B for numerical methods]. For concreteness, throughout the following we consider an initial wave packet that has a Gaussian pro-

file $u(x) = e^{-ikx}e^{-(x-x_0)/2\sigma^2}$. This wave packet is initialized at the center of the periodically wrapped lattice ($x_0 = 0$), with a width one tenth of the width of the lattice ($\sigma = L/10$) and with the same initial velocity ($k_x = \pi/2$) for all simulations. The wave packet evolving under the weakly disordered Hatano-Nelson model Eq. (1) converges to an envelope around the point of maximal amplification k_0 [Fig. 1 (a), red curve], where k_0 is the k-point corresponding to the eigenvalue with the largest positive imaginary part, calculated from the dispersion of the Hamiltonian without disorder. For large disorder, the waveform acquires a non-universal shape whose center of mass is not guaranteed to be located around k_0 [Fig. 1 (a), black curve].

The motion of the center of mass of the waveform in real space defines the drift velocity of the wave packet, $v_{\text{drift}} = \partial_t [\langle\psi|\hat{x}|\psi\rangle/\langle\psi|\psi\rangle]$, with $\hat{x}$ the position operator. We evaluate this expression and obtain:

$$\partial_t [\langle\psi|\hat{x}|\psi\rangle/\langle\psi|\psi\rangle] = \frac{1}{2}\langle\psi|\partial_k\left(H + H^\dagger\right)|\psi\rangle + \frac{i}{2}\langle\psi|\{H - H^\dagger, \langle\psi|\hat{x}|\psi\rangle - \hat{x}\}|\psi\rangle, \quad (2)$$

where $\{\cdot,\cdot\}$ is the anticommutator and where we normalize the wave function such that $\langle\psi|\psi\rangle = 1$. Details of the derivation of Eq. (2) are in Appendix C.

The momentum-space non-Hermitian generalization of the current associated with a Hamiltonian H is defined as $J(H) = -\partial_k H$. The first term of (2) is $\text{Re}(\langle\psi|J|\psi\rangle)$ and for a single Bloch state k_0, $\partial_t \langle\psi|\hat{x}|\psi\rangle_{k_0} = \text{Re}(J)|_{k_0}$. For the Hatano-Nelson Hamiltonian (1),

$$J(H_{\text{HN}}) = \sum_j i\left(-\frac{W}{2}e^{-h} + U_{1,j}\right)|j\rangle\langle j+1| + i\left(\frac{W}{2}e^h - U_{2,j}\right)|j+1\rangle\langle j|. \quad (3)$$

At the localization transition, the drift velocity of the wave packet v_{drift} falls to 0 [Fig. 1 (b)]. We observe that below the localization transition, v_{drift} is finite and $\text{Re}(J)$ at ϵ_{max} is also finite [Fig. 1 (c)], and likewise when the wave packet is localized the $\text{Re}(J)$ at ϵ_{max} is 0 [Fig. 1 (d)]. Finiteness of the drift velocity and $\text{Re}(J)$ at ϵ_{max} are a consequence of the existence of a point gap in the spectrum of the Hamiltonian: a finite area enclosed by the dispersion relation of the Hamiltonian in the complex plane.

Disorder shifts eigenvalues around in the complex plane, resulting in a different eigenstate becoming maximally amplified. Disorder also nontrivially changes the $\text{Re}(J)$ of these eigenvalues. For strong disorder, the maximally amplified eigenstate is generically localized and $\text{Re}(J) = 0$. The maximally amplified state may have nonzero $\text{Re}(J)$ [Fig. 1 (c)], and therefore be delocalized [Fig. 1 (b)] or have zero $\text{Re}(J)$ [Fig. 1 (d)], and therefore be localized [Fig. 1 (b)]. If that state is delocalized, then the system delocalizes. Likewise if it is localized the system is localized even if other states in the systems are delocalized, since these states are always less amplified than the state at ϵ_{max}. Fig. 1 (d) shows that although delocalized states exist for $\epsilon < \epsilon_{\text{max}}$, the system is localized because the maximally amplified state at ϵ_{max} has $\text{Re}(J) = 0$.

3 Transition between propagating phases

The expectation that propagating waveforms in non-Hermitian systems always evolve to the maximally amplified waveform suggests that a transition between competing propagating phases whose ϵ are close to ϵ_{max} should be possible. Here we construct a Hamiltonian with an ∞-shaped dispersion relation that allows to discontinuously switch the velocity of a maximally
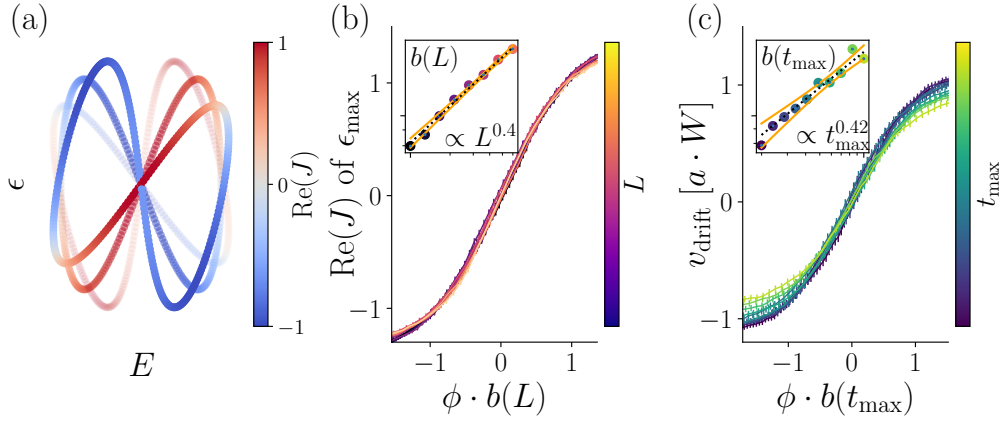
Figure 2: Phase transition between left and right moving wave packets of Hamiltonian H_∞ (4), with onsite and hopping disorder strength in units of the system bandwidth W. Random disorder terms $U_{i,j}$ with $i \in \{0,1,2,3,4\}$ and j the site number (4) are sampled from distributions with standard deviation δ_i. We set $\delta_0 = \delta_1 = \delta_2 = \delta_3 = \delta_4 \equiv \delta = 0.1$. (a) Real-space spectra for $\phi = 0.3$ (most transparent), $\phi = 0$ (intermediate transparency) and $\phi = -0.3$ (most opaque). (b) Rescaled Re(J) of the maximally amplified eigenstate and (c) v_{drift} around $\phi = 0$. Insets: scaling function of the slope at the transition and the 95% confidence interval. Plot details in App. A.

localized wave vector as a function of its parameters [see Fig. 2 (a)]:

$$
H_\infty = \sum_j U_{0,j}|j\rangle\langle j| + \left(\frac{We^{i\phi}}{2}e^{-h} + U_{1,j}\right)|j\rangle\langle j+1| + \left(\frac{We^{i\phi}}{2}e^{h} + U_{2,j}\right)|j+1\rangle\langle j|
$$
$$
+ \left(\frac{We^{i\phi}}{2}e^{-h} + U_{3,j}\right)|j\rangle\langle j+2| + \left(-\frac{We^{i\phi}}{2}e^{h} + U_{4,j}\right)|j+2\rangle\langle j|, \tag{4}
$$

where the sum runs over sites j of the system, W is a hopping parameter that sets the bandwidth of the system, ϕ rotates the spectrum in the complex plane, and where std$(U_{k,j}) = \delta_k$ as in (1). The non-Hermitian generalization of the current J is given by

$$
J(H_\infty) = \sum_j i\left(\frac{We^{i\phi}}{2}e^{-h} + U_{1,j}\right)|j\rangle\langle j+1| + i\left(\frac{We^{i\phi}}{2}e^{h} + U_{2,j}\right)|j+1\rangle\langle j|
$$
$$
+ 2i\left(\frac{We^{i\phi}}{2}e^{-h} + U_{3,j}\right)|j\rangle\langle j+2| - 2i\left(\frac{We^{-i\phi}}{2}e^{h} + U_{4,j}\right)|j+2\rangle\langle j|. \tag{5}
$$

The eigenstates associated to the eigenvalues at the top of the left lobe of the complex dispersion relation propagate to the left, while those at the top of the right lobe propagate right, as shown by the sign of Re(J). By continuously tuning ϕ through 0, there is a discontinuous change in the eigenvalue with the largest positive imaginary component [Fig. 2 (a)] which leads to an abrupt transition between two different maximally amplified eigenstates. When $\phi \neq 0$, wave packets are amplified either predominantly to the left or to the right. The maximally amplified eigenstate of H_∞ at $\phi = 0^-$ propagates to the left, and the one at $\phi = 0^+$ propagates to the right, meaning there is a metal-metal transition at $\phi = 0$. This transition is marked by a switch in the signs of both Re(J) and v_{drift} [Fig. 2 (b)-(c)].

In the presence of disorder and for finite system size, the average of Re(J) at ϵ_{max} and v_{drift} changes linearly in the vicinity of $\phi = 0$, with an intermediate localized point at the middle

Table 1: Scaling parameters of the phase transitions shown in Fig. 2 and 3.

Model	Quantity	Scaling exponent
H_∞ (4)	$\mathrm{Re}(J)$	0.41 ± 0.01
	v_{drift}	0.45 ± 0.03
H_{HN} (1)	v_{drift}	0.38 ± 0.04

of the transition. The slope of this transition increases with system size L (for $\mathrm{Re}(J)$), and the total number of simulated time steps t_{max} (for v_{drift}). We therefore confirm that the transition between the two propagating phases on either side of $\phi = 0$ does not go through a localized phase.

We examine finite-size scaling of the system at the transition. Due to the shape of the spectrum of H_∞ [Fig. 2 (a)] on either side of the transition, the distribution of E is bimodal, grouped around two values where ϵ is the largest. The variance of the individual peaks is the same at the transition point $\phi = 0$. Their standard deviations dictate the width of the transition, as $\phi \cdot t$ is required to be larger than these standard deviations in order for one part of the spectrum, and therefore one value of $\mathrm{Re}(J)$ to 'win' over the other.

There are several considerations we can make in order to estimate the scaling of these standard deviations as a function of system size. The variance of the peak positions equals to the variance of the expectation value of the disorder $U(x)$ in the system, $\mathrm{var}(\langle \psi | U(x) | \psi \rangle) = \mathrm{var}(\int_0^L \psi^*(x) U(x) \psi(x) dx)$. We reach an analytical expression for the scaling of the variance of the peak by assuming that the maximally localized wave packets spread throughout the system on both sides of the transition so that $|\psi| \sim$ const. Therefore the dependence of the variance of the expectation value on system size L is given by $\mathrm{var}(L^{-1} \int_0^L U(x) dx) = L^{-2} \cdot \mathrm{var}\left(\int_0^L U(x) dx\right) \propto L^{-2} L = L^{-1}$. From this we conclude that the standard deviation of each peak of the distribution of ϵ, and therefore the width of the transition, scales with $1/\sqrt{L}$. This leads to the expectation for the finite-size scaling of $b(L)$ to follow $\sqrt{L}$. This estimate differs from the critical exponent $\nu = 1$ [5] of the single energy delocalization transition and suggests that the two transitions are of different nature. This analytical argument relies solely the existence of two non-adjacent maxima of $\mathrm{Im}(E)$, and therefore applies to a broad class of models, suggesting that the metal-metal transition is universal.

To compute the critical exponent from the numerical simulations we fit v_{drift} and $\mathrm{Re}(J)$ of Fig. 2 with the function

$$a \tanh(b\phi), \tag{6}$$

where a and b are functions of system size L for $\mathrm{Re}(J)$ fits, and functions of simulation time t_{max} for v_{drift}. We choose b as our relevant scaling parameter, since it measures the width of the transition. The fitting function $\tanh(b\phi)$ has a discontinuous jump at $L \to \infty$ similar to scaling variables in other systems, such as Hall conductivity σ_{xy} at quantum Hall plateau transitions. The numerical results for $\mathrm{Re}(J)$ at ϵ_{max} show that the critical exponent extracted from the scaling is $\nu \approx 1/2$, as predicted by our analytical estimate [inset of Fig. 2 (c)]. At this moment we cannot deterimne whether the difference of the numerical results and the analytical estimate $\nu = 1/2$ as reported in Table 1 is potentially due to finite-size effects of the simulation or a missing aspect of the analytical estimate. Although we have no analytical argument for the scaling of v_{drift}, it also appears to be closer to $\nu = 1/2$ scaling than $\nu = 1$ scaling [see inset of Fig. 2 (d) and Table 1]. App. D contains further discussion of the bimodal behavior.
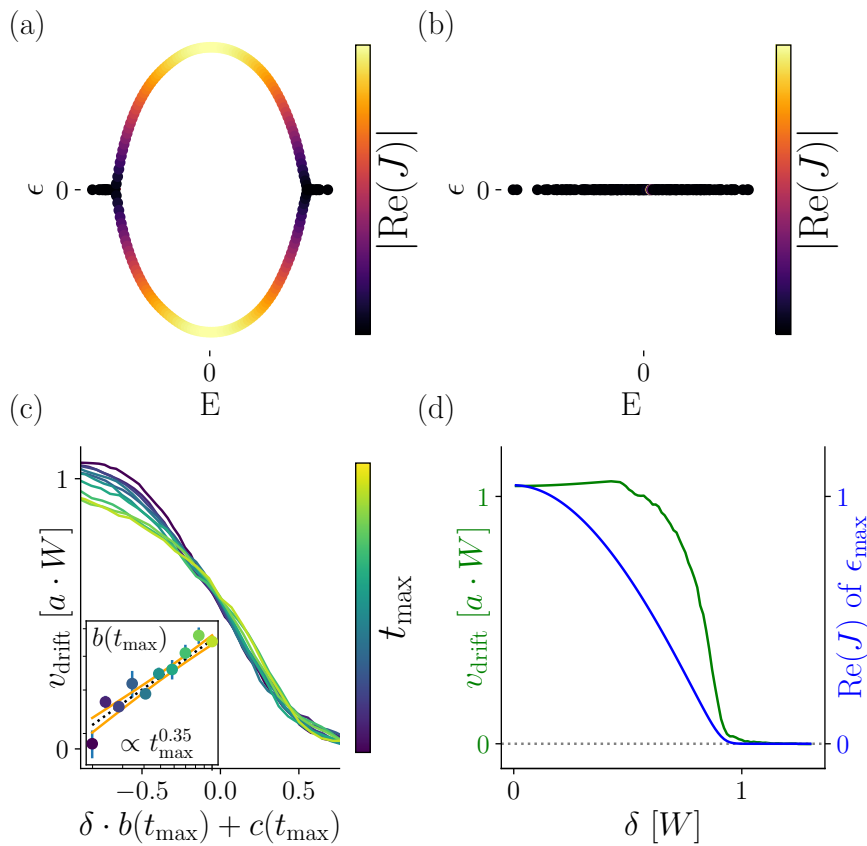
Figure 3: Finite-size scaling of the Hatano-Nelson Hamiltonian Eq. (1), with onsite disorder. Random disorder terms $U_{i,j}$ with $i \in \{0, 1, 2\}$ and j the site number (1) are sampled from distributions with standard deviation δ_i. We set $\delta_1 = \delta_2 = 0$ and label δ_0 as δ. (a)-(b) The Hatano-Nelson spectrum for disorder strength (a) $\delta = 0.3$ and (b) $\delta = 1.2$. (c) Rescaled wave packet drift v_{drift} at the transition point, collapsed using the relevant scaling parameter $b(t_{\text{max}})$ and the irrelevant scaling parameter $c(t_{\text{max}})$. Inset: fit of the scaling parameter $b(t_{\text{max}})$ and the 95% confidence interval. (d) Comparison of v_{drift} (green) to Re(J) of ϵ_{max} (blue) for system sizes $L = 10^3$. Plot details in App. A.

4 Metal-insulator transition

The metal-metal transition behaves differently from the single-frequency response, which raises the question whether the metal-insulator transition is also different. In the presence of non-Hermitian disorder in both the onsite and hopping terms, the metal-insulator transition of the Hatano-Nelson Hamiltonian is the result of a discontinuous change in ϵ_{max} [Fig. 1 (b)-(d)], and the same arguments as the metal-metal transition apply there. We therefore test whether a transition that does not involve a discontinuous switch of ϵ_{max} and E matches the single-frequency response. The original Hatano-Nelson Hamiltonian [3] fulfills this condition. We obtain this Hamiltonian by setting the disorder terms δ_i of Eq. (1) to be 0 except for δ_0. Here the maximally amplified state is the last state to localize, as the mobility edge moves from the largest absolute values of E to the smallest [Fig. 3 (a)-(b)].

The shapes of the $v_{\text{drift}}(\delta)$ curves of Fig. 3 do not lend themselves to a tanh fit. The scaling variable b we choose in this case is the maximum slope during the transition. We also track an irrelevant scaling variable c to ensure the superposition of the rescaled curves. The v_{drift}

curves do not fully collapse at the transition [Fig. 3 (c)]. The scaling of v_{drift} is $b(t_{max}) \propto t_{max}^{0.38}$. We have no analytical expectation for the scaling of v_{drift}, however we cannot rule out that the different critical exponent is due to finite-size effects and a finite resolution of the simulation, as demonstrated by the quality of the fit of the scaling parameter [see inset of Fig. 3 (c)]. The scaling behavior differs from $v = 1$ and is close to $v = 1/2$.

Here Re(J) does not exhibit finite-size scaling and therefore does not show a phase transition. The phase transition of v_{drift} is thus ascribable to the non-linear term of Eq. (2) since it is absent from the linear term. Re(J) and v_{drift} nevertheless both fall to 0 at the same point [Fig. 3 (d)]. When taking the biorthogonal expectation value to calculate Re(J), finite-size scaling does occur [See App. E for discussion].

5 Conclusion

We showed that the dominant dynamics are attributable to a single point in the Fourier space of wave packets, which corresponds to the maximally amplified eigenstate. In the long time limit and in the presence of disorder, wave packets follow a behavior that is independent of initial conditions because they converge to the maximally amplified waveform. Focusing on the metal-metal transition, we presented an analytical argument that yields an expected value of the critical exponent of $v = 1/2$ in any model with two separate maxima of the dispersion relation in the complex plane. For transitions between propagating phases as well as for localization transitions, our numerical results yield $v \approx 1/2$, with deviations from our analytical prediction $v = 1/2$ likely due to finite-size effects. The reasonable agreement between our numerics and our analytical estimate is a strong indication that $v = 1/2$ is universal. Our results clearly prove that wave packet transitions in disordered non-Hermitian media differ from the single-frequency response, $v = 1$.

In our simulations we have observed that drift velocity of a wave packet $v_{drift}(t_{max})$ follows a scaling law similar to the scaling of an eigenstate in a finite system. It is not obvious that this equivalence is guaranteed, and further studies are required.

The nature of transitions in higher-dimensional non-Hermitian systems remains an open question. Preliminary results for two-dimensional systems show that the critical exponent differs from both $v = 1$ and $v = 1/2$ [App. F]. It is therefore likely that the critical exponents of wave packet dynamics in non-Hermitian systems are dimension-dependent.

Non-Hermitian systems are naturally realizable in experiment, and non-Hermitian wave packet dynamics are studied in photonic lattices and electrical circuits [8–10, 10–14]. The transition between propagating phases can be implemented as a switch tuned by a continuous parameter, with uses in control or sensor systems.

Acknowledgments

Data and code availability The data shown in the figures, as well as the code generating all of the data is available at [15].

Author contributions The initial project idea was formulated by I. C. F. and was discussed and later refined with contributions from H. S., V. K., and A. A. Results and code for non-Hermitian spectra were produced by H. S. The initial version of the wave packet propagation code and the error estimation were produced by V. K. Wave packet propagation with disorder was simulated by F. G. under the supervision of H. S. A. A related to relevant literature and formulated the question of comparing wave packet and single frequency phase transitions. The final data was generated by H. S. with input from I. C. F., A. A., and V. K. The scaling analysis was performed by H. S. with guidance from I. C. F. The manuscript was written by H. S. with contributions from I. C. F., A. A., and V. K. The project was managed by H. S. and A. A.

A Model and plotting parameters

For Fig. 1 (b), δ is varied between 0.01 and 0.3 in 50 steps, and the average drift velocity is averaged over 600 different disorder configurations. The spectra of panels (c) and (d) are calculated for systems composed of 300 lattice sites, and parameter h set to 0.3. For panels (a) and (b), the wave packet evolution was performed on system sizes of 600 sites, in steps of $dt = 0.01$ for 60000 steps. For panel (a) the results displayed in the figure are taken at the last step of the time evolution. The disorder strength δ is given in units of W the bandwidth of H_{HN}.

For Fig. 2, the spectra, $\mathrm{Re}(J)$ and the wave packet results are obtained for systems with sizes $L \in \{199, 238, 285, 341, 408, 488, 584, 698, 836, 1000\}$. Results for $\mathrm{Re}(J)$ and wave packets are averaged over 2000 and 500 different disorder configurations respectively. The wave packet evolution was performed in steps of $dt = 0.01$ for L/dt steps. The tilt angle ϕ was varied between -0.1 and 0.1 in the following way: 20 points between -0.1 and -0.03, 100 points between -0.03 and 0.03, and 20 between 0.03 and 0.1. The disorder strength is set to $\delta = 0.1$ in units of the bandwidth W of the Hamiltonian Eq. (4).

For Fig. 3, the parameter h is set to 0.3. Ten different system sizes L are simulated, $L \in \{199, 238, 285, 341, 408, 488, 584, 698, 836, 1000\}$. Results are averaged over 500 different disorder configurations for each value of disorder strength. The wave packet evolution was performed in steps of $dt = 0.01$ for L/dt steps, with the values of L as stated above.

For the insets of Fig. 2 (b)-(c) and Fig. 3 (c), the error of the scaling fit is shown using the 95% confidence interval.

For Fig. 4, panel (a) data is made up of 5000 disorder configurations, for systems 800 sites long. Panel (c) data is made up of 3000 disorder configurations, for systems 800 sites long. Panel (c) data is made up of 2000 disorder configurations, for systems 1000 sites long. Panel (d) data is made up of 3000 disorder configurations, for systems 800 sites long and $\delta = 0.8$. The wave packet results are obtained for time evolution step size $dt = 0.01$ and total time steps L/dt.

Fig. 7 is composed of unscaled data that was obtained and used in Fig. 2 and Fig. 3.

For Fig. 6, the wave packet evolution was performed in steps of $dt = 0.01$ for L/dt steps. Five different system sizes $L \times L$ were simulated, with $L \in \{64, 85, 113, 150, 199\}$. Disorder strengths were varied between 0.01 and 0.5 in 50 steps. For each disorder strength, the result is averaged over 400 different disorder configurations.

For Fig. 5, panel (a) data for $\delta = 0.01$ is composed of 100 different disorder configurations for systems of 800 sites. Panel (a) data for $\delta = 0.1$ is made up of 1000 disorder

configurations, for systems 1000 sites long. Panel (b) data is made up of 5000 disorder configurations, for systems 800 sites long and $\delta = 0.8$. For panel (c), results for Re(J) and wave packets are averaged over 500 different disorder configurations. The tilt angle ϕ was varied between -0.1 and 0.1 in the following way: 20 points between -0.1 and -0.03, 100 points between -0.03 and 0.03, and 20 between 0.03 and 0.1. Results are obtained for systems with sizes $L \in \{199, 238, 285, 341, 408, 488, 584, 698, 836, 1000\}$. The disorder strength is set to $\delta = 0.1$ in units of the bandwidth W of the Hamiltonian (4). For the insets of panels (c)-(d), the error of the scaling fit is shown using the 95% confidence interval.

B Numerical methods

The time evolution of the wave packets was calculated using the scaled Taylor expansion method to first order [16–18], obtaining

$$|\psi(t + dt)\rangle = |\psi(t)\rangle - iH|\psi(t)\rangle dt, \tag{B.1}$$

where $|\psi(t)\rangle$ is the wave function at time t, dt is the time step, and H is the Hamiltonian dictating the time evolution. The simulation time t and timesteps dt are in units of the bandwidth W of the system. We choose $dt = 0.01$, but we have separately checked that our results hold also for smaller time steps. In our simulations we initialize the system from the same real-space Gaussian wave packet. In order to ensure that the wave packets do not reach the system boundary, we limit the total number of time steps used for a simulation to $t_{\max} = L/(a \cdot dt \cdot v_{\mathrm{drift}})$, with L the system size, a the lattice constant and v_{drift} the drift velocity of the wave packet for low disorder. Above the localization transition, $t_{\max}$ is not shortened in order to record instances of 'teleportation' of the drift center of the maximally amplified wave packet, which contribute to the average velocity.

The method is based on the following expression for the matrix exponential

$$e^{-itH} = \lim_{N \to \infty} \left(I - \frac{itH}{N} \right)^N, \tag{B.2}$$

where N is the number of time steps. Fixing the time step ($dt = t/N$) and the number of steps (N) we get an approximation for the time evolution operator as:

$$e^{-itH} \approx (I - idtH)^N. \tag{B.3}$$

The error introduced at each subsequent time step can be estimated using the errors calculated for Taylor polynomials of the first order as [17, 18]:

$$\delta = \left\| e^{-idtH} - I + idtH \right\| \leq \frac{dt^2 \|H\|^2}{2} \frac{1}{1 - \frac{dt\|H\|}{3}}, \tag{B.4}$$

where $\|\cdot\|$ is any well defined matrix norm, for simplicity we use the spectral norm. For normalized Hamiltonians $\|H\| = 1$ and $dt \leq 1$, the error introduced at each time step is $\delta \leq 3dt^2/4$.

C Analytical form of wave packet center of mass drift velocity

In this section we provide details concerning the derivation of Eq. (2).

Starting from $\partial_t[\langle\psi|\hat{x}|\psi\rangle/\langle\psi|\psi\rangle]$ and using the quotient rule,

$$\partial_t[\langle\psi|\hat{x}|\psi\rangle/\langle\psi|\psi\rangle] = \frac{\partial_t[\langle\psi|\hat{x}|\psi\rangle] \cdot \langle\psi|\psi\rangle}{\langle\psi|\psi\rangle^2} - \frac{\langle\psi|\hat{x}|\psi\rangle \cdot \partial_t[\langle\psi|\psi\rangle]}{\langle\psi|\psi\rangle^2}. \tag{C.1}$$

We first calculate $\partial_t[\langle\psi|\psi\rangle]$. Using

$$|\psi\rangle = e^{-itH}|0\rangle\,, \tag{C.2}$$

$$\langle\psi| = \langle 0|e^{itH^\dagger}\,, \tag{C.3}$$

we find

$$\partial_t[\langle\psi|\psi\rangle] = \partial_t[\langle 0|e^{itH^\dagger}e^{-itH}|0\rangle] \tag{C.4}$$

$$= \langle 0|iH^\dagger e^{itH^\dagger}e^{-itH}|0\rangle + \langle 0|e^{itH^\dagger}(-iH)e^{-itH}|0\rangle \tag{C.5}$$

$$= i\langle\psi|H^\dagger - H|\psi\rangle\,. \tag{C.6}$$

Similarly for $\partial_t[\langle\psi|\hat{x}|\psi\rangle]$,

$$\partial_t[\langle\psi|\hat{x}|\psi\rangle] = \partial_t[\langle 0|e^{itH^\dagger}\hat{x}e^{-itH}|0\rangle] \tag{C.7}$$

$$= \langle 0|iH^\dagger e^{itH^\dagger}\hat{x}e^{-itH}|0\rangle + \langle 0|e^{itH^\dagger}\hat{x}(-iH)e^{-itH}|0\rangle \tag{C.8}$$

$$= i\langle\psi|H^\dagger\hat{x} - \hat{x}H|\psi\rangle\,. \tag{C.9}$$

Substituting these expressions into Eq. (C.1), we obtain

$$\partial_t[\langle\psi|\hat{x}|\psi\rangle/\langle\psi|\psi\rangle] = i\langle\psi|H^\dagger\hat{x} - \hat{x}H|\psi\rangle - i\langle\psi|\hat{x}|\psi\rangle\langle\psi|H^\dagger - H|\psi\rangle\,, \tag{C.10}$$

where we use that $\langle\psi|\psi\rangle = 1$.

We then express Eq. (C.10) in terms of the current operator $J = i[H,\hat{x}]$. Using

$$\mathrm{Re}(J) = -\mathrm{Im}([H,\hat{x}]) = \frac{i}{2}(\langle\psi|[H,\hat{x}]|\psi\rangle - \langle\psi|[\hat{x},H^\dagger]|\psi\rangle) \tag{C.11}$$

$$= \langle\psi|(H\hat{x} - \hat{x}H - \hat{x}H^\dagger + H^\dagger\hat{x})|\psi\rangle\,, \tag{C.12}$$

we obtain

$$\partial_t[\langle\psi|\hat{x}|\psi\rangle/\langle\psi|\psi\rangle] = \mathrm{Re}(J) + \frac{i}{2}\langle\psi|(H^\dagger\hat{x} - \hat{x}H - H\hat{x} + \hat{x}H^\dagger)|\psi\rangle - i\langle\psi|\hat{x}|\psi\rangle\langle\psi|H^\dagger - H|\rangle\,. \tag{C.13}$$

We rewrite the second and third terms of Eq. (C.13) as

$$\partial_t[\langle\psi|\hat{x}|\psi\rangle/\langle\psi|\psi\rangle] = \mathrm{Re}(J) + \frac{i}{2}\langle\psi|(H^\dagger\hat{x} - \hat{x}H - H\hat{x} + \hat{x}H^\dagger + 2\langle\psi|\hat{x}|\psi\rangle(H - H^\dagger))|\psi\rangle \tag{C.14}$$

$$= \mathrm{Re}(J) + \frac{i}{2}\langle\psi|((H - H^\dagger)(2\langle\psi|\hat{x}|\psi\rangle - \hat{x}) - \hat{x}(H - H^\dagger))|\psi\rangle \tag{C.15}$$

$$= \mathrm{Re}(J) + \frac{i}{2}\langle\psi|((H - H^\dagger)(\langle\psi|\hat{x}|\psi\rangle - \hat{x}) - (\langle\psi|\hat{x}|\psi\rangle - \hat{x})(H - H^\dagger))|\psi\rangle \tag{C.16}$$

$$= \mathrm{Re}(J) + \frac{i}{2}\langle\psi|\{(H - H^\dagger),(\langle\psi|\hat{x}|\psi\rangle - \hat{x})\}|\psi\rangle\,. \tag{C.17}$$

D Multimodal behavior

Here we discuss the shape of the distributions of $\mathrm{Re}(J)$ and v_{drift} of both the H_∞ [Eq. (4)] and H_{HN} [Eq. (1)] models around the transition point.
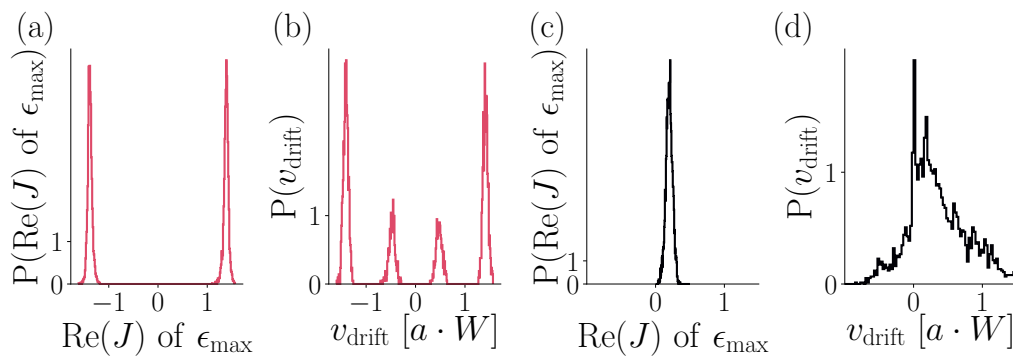
Figure 4: Multimodal and bimodal distributions of $\mathrm{Re}(J)$ and v_{drift} of the Hamiltonians H_∞ [Eq. (4)] and H_{HN} [Eq. (1)]. For the Hatano-Nelson Hamiltonian (1), random disorder terms $U_{i,j}$ with $i \in \{0, 1, 2\}$ and j the site number are sampled from distributions with standard deviation δ_i. We set $\delta_0 = \delta_1 = \delta_2 \equiv \delta$. For the Hamiltonian H_∞ (4), random disorder terms $U_{i,j}$ with $i \in \{0, 1, 2, 3, 4\}$ and j the site number are sampled from distributions with standard deviation δ_i. We set $\delta_0 = \delta_1 = \delta_2 = \delta_3 = \delta_4 \equiv \delta$. (a), (c) distributions of $\mathrm{Re}(J)$ of the maximally amplified state and v_{drift} of the H_∞ model at $\phi = 0$ and $\delta = 0.1$. (b), (d) distributions of $\mathrm{Re}(J)$ of the maximally amplified state and v_{drift} of the H_{HN} model at $\phi = 0$ and $\delta = 0.8$. Plot details in App. A.

For H_∞, the distribution of $\mathrm{Re}(J)$ of the maximally amplified eigenstate is bimodal [Fig. 4 (a)]. The distribution of v_{drift} is multimodal [Fig. 4 (c)]. The multimodality arises from the disorder nontrivially shifting eigenvalues of H_∞ in the complex plane, creating two bimodal distributions for v_{drift}, one on each side of the transition in ϕ. The same multimodal behavior is seen in $\mathrm{Re}(J)$ of the maximally amplified eigenstate when using biorthogonal expectation values to calculate J [App. E, Fig. 5 (a)].

For H_{HN}, $\mathrm{Re}(J)$ does not exhibit a transition [Fig. 3 (d)], and its distribution close to the v_{drift} transition is centered around a small but finite value [Fig. 4 (b)]. The scaling of v_{drift} of the Hatano-Nelson model H_{HN} does not exactly follow $\sqrt{t_{\mathrm{max}}}$ [Table 1 and Fig. 3 (d)] but a bimodal distribution is still observed close to the transition [Fig. 4 (d)]. Close to the transition point, the distribution of v_{drift} has two peaks, with one broad peak centered around a finite value, and the other delta function peak around 0. The v_{drift} around 0 originates from disorder configurations that result in localization, and the v_{drift} with finite velocity originates from disorder configurations where propagation is still possible.

E   Biorthogonal expectation value

In the results of the manuscript, we calculated $\mathrm{Re}(J)$ of the state m as $\mathrm{Re}(\langle\psi_m|J|\psi_m\rangle)$ such that $\langle\psi_m| = |\psi_m\rangle^\dagger$. In this section we calculate $\mathrm{Re}(J)$ of state m as $\mathrm{Re}(\langle\psi_m|J|\psi_m\rangle)$ such that $\langle\psi_m| = |\psi_m\rangle^{-1}$, that is to say $\langle\psi_m|$ is the m-th left eigenstate and $|\psi_m\rangle$ is the m-th right eigenstate. We refer to this $\mathrm{Re}(\langle\psi_m|J|\psi_m\rangle)$ as the biorthogonal expectation value of $\mathrm{Re}(J)$. The behavior of $\mathrm{Re}(J)$ is significantly impacted by this change in expectation value, as shown in Fig. 5.

For the H_∞ model, similarly to Fig. 4 for low disorder ($\delta = 0.01$) the distribution of $\mathrm{Re}(J)$ of the maximally amplified eigenstate is bimodal [Fig. 5 (a)]. At finite disorder, the distribution becomes multimodal, similar to v_{drift} [Fig. 4 (c)]. The scaling parameter at the transition of the biorthogonally projected $\mathrm{Re}(J)$ scales as $L^{0.44\pm0.01}$ [Fig. 5 (c)].
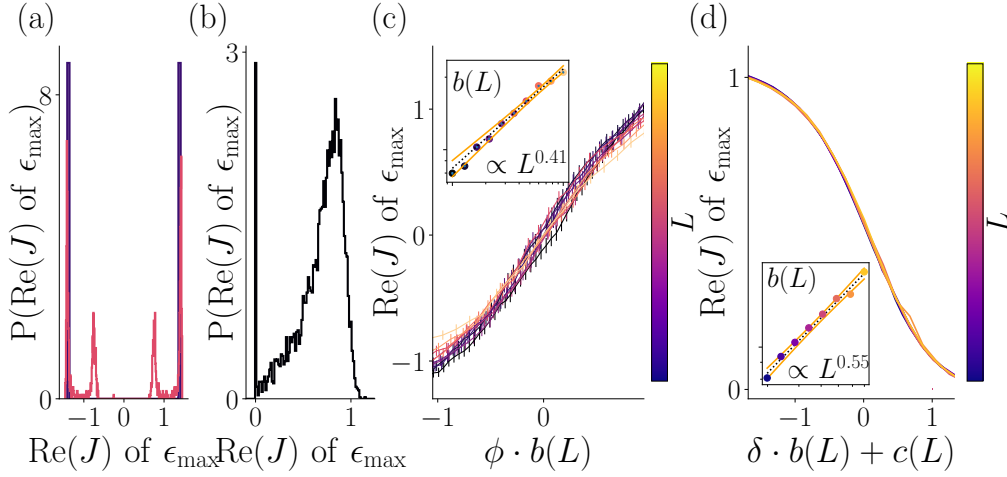
Figure 5: $\text{Re}(J)$ results using biorthogonal expectation values for Hamiltonians H_∞ [Eq. (4)] and H_{HN} [Eq. (1)]. For the Hatano-Nelson Hamiltonian (1), random disorder terms $U_{i,j}$ with $i \in \{0,1,2\}$ and j the site number are sampled from distributions with standard deviation δ_i. We set $\delta_0 = \delta_1 = \delta_2 \equiv \delta$. For the Hamiltonian H_∞ (4), random disorder terms $U_{i,j}$ with $i \in \{0,1,2,3,4\}$ and j the site number are sampled from distributions with standard deviation δ_i. We set $\delta_0 = \delta_1 = \delta_2 = \delta_3 = \delta_4 \equiv \delta$. (a) distributions of $\text{Re}(J)$ of the maximally amplified state of the H_∞ model at $\phi = 0$ and $\delta = 0.1$ and $\delta = 0.01$ in units of the bandwidth W. (b) distribution of $\text{Re}(J)$ of the maximally amplified state of the H_{HN} model at $\delta = 0.8$. (c) Rescaled $\text{Re}(J)$ of the maximally amplified state of the H_∞ model for $\delta = 0.1$. (d) Rescaled $\text{Re}(J)$ of the maximally amplified state of the H_{HN} model for $\delta = 0.1$. Insets of (c) and (d): scaling functions of the slope at the transition and the 95% confidence interval. Plot details in App. A.

The Hatano-Nelson model H_{HN} also exhibits bimodal behavior [Fig. 5 (b)], similarly to the distribution of v_{drift} [Fig. 4 (d)]. Close to the transition point, the distribution of $\text{Re}(J)$ has two peaks, with one broad peak around the low-disorder $\text{Re}(J)$ value 1.1, and the other delta function peak around the high disorder $\text{Re}(J)$ value 0. In the biorthogonal case, the $\text{Re}(J)$ of the H_{HN} displays a phase transition. The scaling of the transition width is found to scale close to $\sqrt{L}$, as $L^{0.55\pm0.02}$ [Fig. 5 (d)], similarly to the H_∞ case.

The $\text{Re}(J)$ calculated using the biorthogonal expectation value appears to follow the behavior of v_{drift} more closely, but we do not have an argument as to why this would be the case.

F Results in two dimensions

We consider the following two-dimensional non-Hermitian model:

$$H_N = \sum_{d=1}^{N} \sum_{j}^{L_d} U_{0,j} |x_{d,j}\rangle\langle x_{d,j}| + \left(t_{x_d,+} + it'_{x_d,+} U_{1,d,j}\right) |x_{d,j+1}\rangle\langle x_{d,j}|$$
$$+ \left(t_{x_d,-} + it'_{x_d,-} + U_{2,d,j}\right) |x_{d,j}\rangle\langle x_{d,j+1}|, \tag{F.1}$$

where the sum runs over all the lattice sites j and the spatial dimensions d of a N-dimensional system with $L/a = \frac{1}{a}\sum_d^N L_d$ sites, with a the lattice constant. x_d corresponds to the spatial

Table 2: Parameters used for simulating Hamiltonian Eq. (F.1).

Parameter	value
$t_{x,+}$	1
$t'_{x,+}$	0
$t_{x,-}$	0.8
$t'_{x,-}$	0
$t_{y,+}$	0
$t'_{y,+}$	0
$t_{y,-}$	0
$t'_{y,-}$	1

coordinate in dimension d, and $U_{n,d,j}$ are random disorder terms sampled from a distribution $\delta_{n,d}$. We choose $N = 2$.

The parameters we use in simulating this model are found in Table 2, and yield the spectrum shown in Fig. 6 (a)-(b). Wave packets are initialized at the center of the periodically wrapped lattice ($x_0 = [0,0]$), with a width one tenth of the width of the lattice ($\sigma = L/10$) and with the same initial velocity ($k_x = \pi/2, k_y = 0$) for all simulations.

We fit the function $a \tanh(b\delta + c)$ to the localization transition of v_{drift} as a function of δ, and extract $b(t_{\text{max}})$. $b(t_{\text{max}})$ scales as $t_{\text{max}}^{0.63 \pm 0.05}$ [Fig. 6 (d)], which differs from the 1D critical exponents presented in the main text [Table 1]. It is not possible from these results to say whether the critical exponent of non-Hermitian systems is dimension-dependent or not.
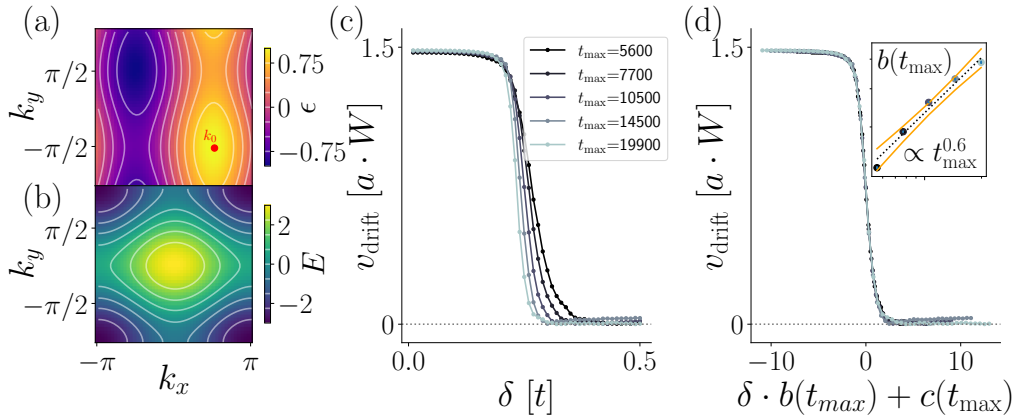

Figure 6: Finite-time scaling of two-dimensional non-Hermitian model Eq. (F.1) with parameters 2. (a)-(b) The Brillouin zone of (a) the imaginary part of the energy ϵ and (b) the real part of the energy. (c) The unscaled localization transition of v_{drift} as a function of disorder. Random disorder terms $U_{i,d,j}$ with $i \in \{0,1,2\}$, $d \in \{x,y\}$ and j the site number (F.1) are sampled from distributions that all have a standard deviation of $\delta_0 = \delta_1 = \delta_2 \equiv \delta$. (d) The rescaled curves of (c). Inset: scaling of the sharpness of the transition. Plot details in App. A.
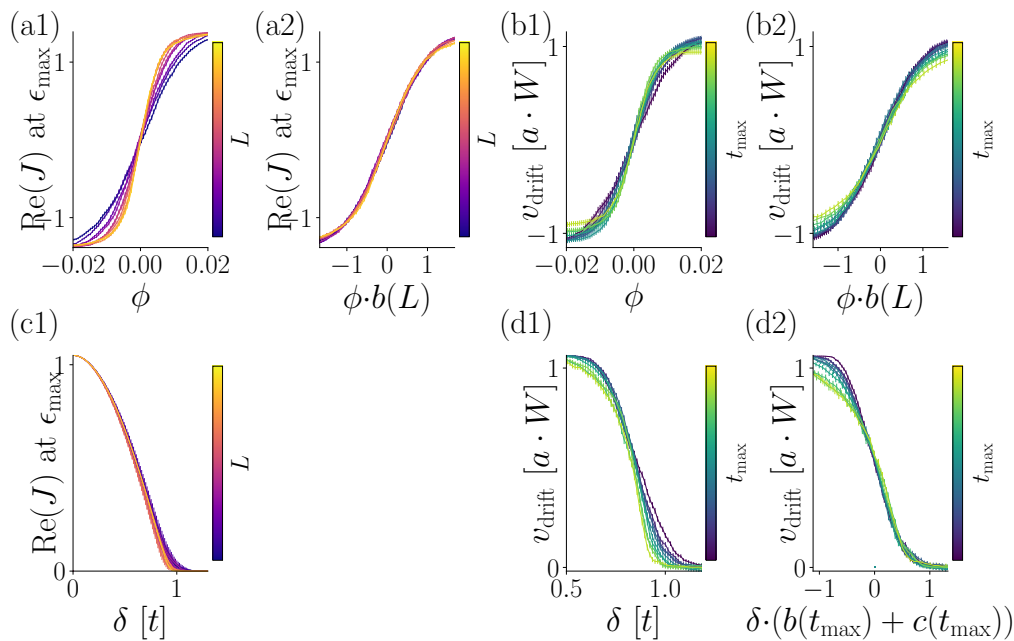
Figure 7: Unscaled (a1,b1,c1,d1) and rescaled (a2,b2,d2) Re(J) at the point of maximal amplification $\epsilon_{\max}$ and v_{drift} at the transition point, as a function of ϕ the tilt angle of the spectrum or as a function of disorder δ. For the Hatano-Nelson Hamiltonian (1), random disorder terms $U_{i,j}$ with $i \in \{0,1,2\}$ and j the site number are sampled from distributions with standard deviation δ_i. We set $\delta_0 = \delta_1 = \delta_2 \equiv \delta$. For the Hamiltonian H_∞ (4), random disorder terms $U_{i,j}$ with $i \in \{0,1,2,3,4\}$ and j the site number are sampled from distributions with standard deviation δ_i. We set $\delta_0 = \delta_1 = \delta_2 = \delta_3 = \delta_4 \equiv \delta$. (a1)-(b2) Results for the H_∞ model Eq. (4) used in Fig. 2. (c1)-(d2) Results for the H_{HN} model Eq. (1) used in Fig. 3. Plot details in App. A.

G Unscaled results

The results for Re(J) at $\epsilon_{\max}$ and v_{drift} shown in Fig. 2 and Fig. 3 are rescaled by the scaling variables b (and c in the case of v_{drift}). Fig. 7 contains the unscaled data used to obtain Fig. 2 and Fig. 3, as well as the rescaled data for comparison.

We do not show rescaling of the Re(J) at $\epsilon_{\max}$ curves of Fig. 7 (c1), since they do not exhibit scaling.

References

[1] P. W. Anderson, *Absence of diffusion in certain random lattices*, Phys. Rev. **109**, 1492 (1958), doi:10.1103/PhysRev.109.1492.

[2] F. Evers and A. D. Mirlin, *Anderson transitions*, Rev. Mod. Phys. **80**, 1355 (2008), doi:10.1103/RevModPhys.80.1355.

[3] N. Hatano and D. R. Nelson, *Localization transitions in non-Hermitian quantum mechanics*, Phys. Rev. Lett. **77**, 570 (1996), doi:10.1103/PhysRevLett.77.570.

[4] P. W. Brouwer, P. G. Silvestrov and C. W. J. Beenakker, *Theory of directed localization in one dimension*, Phys. Rev. B **56**, R4333 (1997), doi:10.1103/PhysRevB.56.R4333.

[5] K. Kawabata and S. Ryu, *Nonunitary scaling theory of non-Hermitian localization*, Phys. Rev. Lett. **126**, 166801 (2021), doi:10.1103/PhysRevLett.126.166801.

[6] K. Kawabata, M. Sato and K. Shiozaki, *Higher-order non-Hermitian skin effect*, Phys. Rev. B **102**, 205118 (2020), doi:10.1103/PhysRevB.102.205118.

[7] H. Sahoo, R. Vijay and S. Mujumdar, *Anomalous transport regime in non-Hermitian, Anderson-localizing hybrid systems*, Phys. Rev. Res. **4**, 043081 (2022), doi:10.1103/PhysRevResearch.4.043081.

[8] P. Zhu, X.-Q. Sun, T. L. Hughes and G. Bahl, *Higher rank chirality and non-Hermitian skin effect in a topolectrical circuit*, Nat. Commun. **14**, 720 (2023), doi:10.1038/s41467-023-36130-x.

[9] M. Wu et al., *Evidencing non-Bloch dynamics in temporal topolectrical circuits*, Phys. Rev. B **107**, 064307 (2023), doi:10.1103/PhysRevB.107.064307.

[10] Q. Lin, T. Li, L. Xiao, K. Wang, W. Yi and P. Xue, *Observation of non-Hermitian topological Anderson insulator in quantum dynamics*, Nat. Commun. **13**, 3229 (2022), doi:10.1038/s41467-022-30938-9.

[11] S. O. Peatáin, T. Dixon, P. J. Meeson, J. Williams, S. Kafanov and Y. A. Pashkin, *The effect of parameter variations on the performance of the Josephson travelling wave parametric amplifiers*, (arXiv preprint) doi:10.48550/arXiv.2112.07766.

[12] S. Weidemann, M. Kremer, S. Longhi and A. Szameit, *Non-Hermitian Anderson transport*, in *Conference on lasers and electro-optics*, Institute of Electrical and Electronic Engineers, New York, USA, ISBN 9781943580767 (2020), doi:10.1364/CLEO_QELS.2020.FTu3A.3.

[13] T. Jiang, A. Fang, Z.-Q. Zhang and C. T. Chan, *Anomalous Anderson localization behavior in gain-loss balanced non-Hermitian systems*, Nanophotonics **10**, 443 (2020), doi:10.1515/nanoph-2020-0306.

[14] F. Noronha, J. A. S. Lourenço and T. Macrì, *Robust quantum boomerang effect in non-Hermitian systems*, Phys. Rev. B **106**, 104310 (2022), doi:10.1103/PhysRevB.106.104310.

[15] H. Spring, V. Konye, F. A. Gerritsma, I. C. Fulga and A. R. Akhmerov, *Phase transitions of wave packet dynamics in disordered non-Hermitian systems*, Zenodo (2023), doi:10.5281/zenodo.7535012.

[16] N. J. Higham, *Functions of matrices: Theory and computation*, SIAM, Philadelphia, USA, ISBN 9780898716467 (2008).

[17] M. L. Liou, *A novel method of evaluating transient response*, Proc. IEEE **54**, 20 (1966), doi:10.1109/PROC.1966.4569.

[18] C. Moler and C. Van Loan, *Nineteen dubious ways to compute the exponential of a matrix, twenty-five years later*, SIAM Rev. **45**, 3 (2003), doi:10.1137/S00361445024180.